Nanoscale Advances

PAPER

View Article Online
View Journal | View Issue

Cite this: *Nanoscale Adv.*, 2019, **1**, 2348

Indirect magnetic force microscopy†

Joshua Sifford,‡[a] Kevin J. Walsh,‡[b] Sheng Tong,[c] Gang Bao[c] and Gunjan Agarwal *[d]

Magnetic force microscopy (MFM) is an atomic force microscopy (AFM)-based technique to map magnetic domains in a sample. MFM is widely used to characterize magnetic recording media, magnetic domain walls in materials, nanoparticles and more recently iron deposits in biological samples. However, conventional MFM requires multiple scans of the samples, suffers from various artifacts and is limited in its capability for multimodal imaging or imaging in a fluid environment. We propose a new modality, namely indirect magnetic force microscopy (ID-MFM), a technique that employs an ultrathin barrier between the probe and the sample. Using fluorescently conjugated superparamagnetic nanoparticles, we demonstrate how ID-MFM can be achieved using commercially available silicon nitride windows, MFM probes and AFM equipment. The MFM signals obtained using ID-MFM were comparable to those obtained using conventional MFM. Further, samples prepared for ID-MFM were compatible with multi-modal imaging *via* fluorescence and transmission electron microscopy. Thus ID-MFM can serve as a high-throughput, multi-modal microscopy technique which can be especially attractive for detecting magnetism in nanoparticles and biological samples.

Received 29th March 2019
Accepted 3rd May 2019

DOI: 10.1039/c9na00193j

rsc.li/nanoscale-advances

Introduction

Magnetic force microscopy (MFM) is a scanning probe microscopy-based technique which enables spatial mapping of magnetic domains on a sample surface.[1] Although MFM was initially limited to characterization of solid-state devices, recent years have witnessed a growing use of MFM to study various kinds of magnetic nanoparticles *in vitro* and iron deposits in biological samples. MFM has been utilized to characterize a variety of magnetic nanoparticles[2–4] and decipher between magnetic and non-magnetic nanoparticles.[5] For superparamagnetic nanoparticles, MFM has been especially useful to evaluate magnetic moment,[6,7] magnetic anisotropy,[8] magnetization curves[9] and the effect of aggregation[10,11] in particles. Applications of MFM have also extended to evaluate biological samples[12] such as ferritin proteins,[13,14] cells labeled with magnetic particles,[15] and magnetic (iron) deposits in bacteria[16,17] and in mammalian tissues.[18,19]

In its most conventional format, the MFM technique employs a magnetically coated probe to scan a sample in the non-contact or dynamic mode of scanning probe microscopy. This method involves tracking the sample topography in which the probe directly touches the sample. Several interleaved scans at various lift heights "*z*" above the topographic height are then obtained to detect the long-range magnetic forces present between the MFM probe and magnetic domains on the sample (Fig. 1a). In the case of superparamagnetic particles, the MFM probe is used to both induce as well as detect magnetic moments in the particles. Since in conventional MFM, the probe directly touches the sample to obtain its topography and thereby ascertain lift height, we hereby use the term 'direct-MFM' or D-MFM to describe this conventional mode of MFM.

D-MFM can be performed on most commercially available atomic force microscopes (AFMs) and is capable of high spatial resolution as well as sensitivity to detect nanoscale magnetic domains even with weak magnetic moments. However, D-MFM has three major limitations that curtail its efficacy and versatility for analysis of magnetic signals from nanoparticles and biological samples. These include: (1) direct contact with the sample can damage or contaminate the probe especially when used for loosely adhered nanoparticles or sticky materials such as biological samples. (2) The probe-sample interaction not only is composed of magnetic forces but can also include a contribution from sample topography, van der Waal interactions and electrostatic forces. As a result, multiple scans at increasing lift-heights or other strategies need to applied,[20,21] thus making the D-MFM technique a time consuming and low-throughput approach. Finally (3) D-MFM is typically limited to imaging in ambient air and not easily amenable to a liquid environment,[22] as immersing the MFM cantilever-probe can significantly dampen the Q-factor of the cantilever, thus decreasing its force sensitivity.

We propose here a novel method which we call 'indirect magnetic force microscopy' (ID-MFM) (Fig. 1b) which builds

[a]*Department of Mechanical Engineering, The Ohio State University, Columbus, OH 43210, USA*

[b]*Biophysics Program, The Ohio State University, Columbus, OH 43210, USA*

[c]*Department of Bioengineering, Rice University, Houston, Texas 77005, USA*

[d]*Department of Biomedical Engineering, The Ohio State University, 288 Bevis Hall, 1080 Carmack Road, Columbus, OH 43210, USA. Fax: +1 614 247 7799; Tel: +1 614 292 4213. E-mail: agarwal.60@osu.edu*

† Electronic supplementary information (ESI) available. See DOI: 10.1039/c9na00193j

‡ These authors contributed equally to this manuscript.

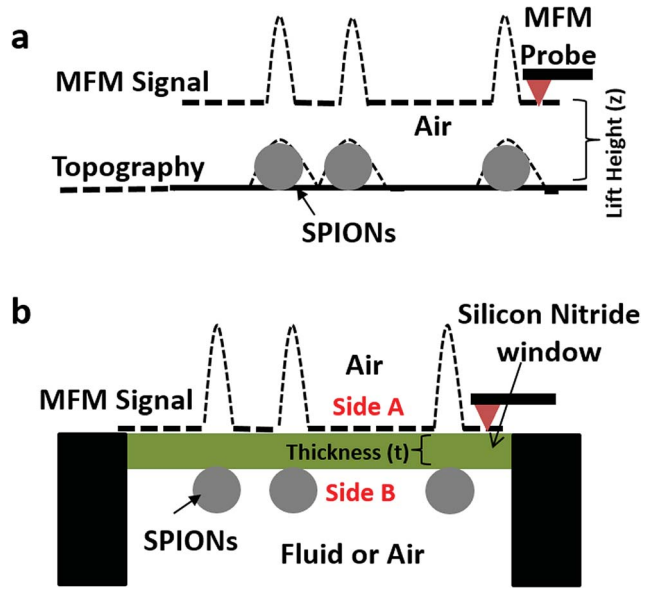

Fig. 1 Schematic of: (a) conventional or direct magnetic force microscopy (D-MFM). In D-MFM the sample (*e.g.* superparamagnetic iron oxide nanoparticles (SPIONs)) topography is tracked by an MFM probe and several scans are acquired at varying lift heights (z). (b) In Indirect MFM (ID-MFM) an ultrathin silicon nitride window of thickness (t) separates the sample and the probe. The MFM signal is obtained by directly scanning the side A of the window.

on the strengths of D-MFM but is geared to overcome its drawbacks. In ID-MFM an ultrathin silicon-nitride window is used to create a physical barrier between the sample and the probe. The window prevents direct contact between the sample and the probe thus protecting against probe contamination. Furthermore, the window eliminates the short-range probe-sample interactions present in D-MFM while enabling long-range magnetic interactions to be detected, thus eliminating the need for multiple scans. In principle, ID-MFM can be performed with the sample in a liquid environment and with the probe in air making it an attractive modality for MFM in fluids. Finally, ID-MFM is amenable to multi-modal imaging and like D-MFM can be performed on most commercial AFM systems.

In this study, we demonstrate the feasibility of ID-MFM to detect magnetic signals from fluorescently conjugated superparamagnetic iron oxide nanoparticles (SPIONs) immobilized on silicon nitride windows. Quantitative analysis of D-MFM and ID-MFM signals enabled a comparison between the two modalities. Measurements using non-magnetic AFM probes were performed in direct and indirect modes to ascertain the specificity of magnetic signal. The multi-modal capability of ID-MFM was evaluated by examining the samples using transmission electron microscopy (TEM) and fluorescence microscopy.

Experimental

Chemical reagents

Iron acetylacetonate ($Fe(acac)_3$ 99%), 1,2-tetradecanediol (technical grade, 90%), oleic acid (technical grade, 90%), oleylamine (technical grade, 70%), benzyl ether (98%), and 1,1′-dioctadecyl-3,3,3′,3′-tetramethylindocarbocyanine perchlorate (DiI) were purchased from Sigma-Aldrich. 1,2-Distearoyl-sngly-cero-3-phosphoethanolamine-*N*-[methoxy(polyethylene glycol)-2000] (ammonium salt) (DSPE-PEG2000) were purchased from Avanti Polar Lipids. All chemicals were used as received.

Synthesis of iron oxide superparamagnetic nanoparticles (SPIONs)

Superparamagnetic iron oxide nanoparticles (SPIONs) of ~15 nm in diameter were synthesized by thermal-decomposition of $Fe(acac)_3$ in a mixture of 1,2-tetradecanediol, oleic acid, oleylamine and benzyl ether according to a published protocol.[23] As-synthesized nanocrystals were dispersed in toluene. To generate water-dispersible SPIONs conjugated to a fluorescent moiety, the nanocrystals were coated with DSPE-PEG2000 *via* a dual-solvent exchange method.[24] Coated SPIONs were mixed with DiI at a ratio of 50 : 1 (Fe : DiI, w/w). Unbound DiI was removed by ultracentrifugation.

SQUID magnetometry

Magnetic properties of SPIONs were measured using a superconducting quantum interference device (SQUID, MPMS, Quantum Design) in a field of −0.5 to 0.5 T at room temperature. Magnetization curves were obtained for uncoated and DSPE-PEG2000 coated SPIONs by dispersing them in hexatriacontane or gypsum respectively, to reduce inter-particle interactions. After the measurements, the iron content of the samples was measured using a ferrozine assay.[23] All measurements were corrected for the background signal from the matrix and normalized by the iron content of the samples.

Magnetic force microscopy

For D-MFM, an aliquot of the SPIONs was dispersed on freshly cleaved mica, blotted and air dried. The mica substrate was adhered to a stainless-steel stub and mounted in the base of a JV scanner. Images were acquired in tapping mode by using a Multimode AFM equipped with a Nanoscope III a controller (Bruker). A scan speed of 2 Hz was used with 512 lines per scan direction. Magnetically coated high-moment MFM probes (ASYMFMHM, Asylum Research) were used to scan the samples. Topographic (height) and phase images were acquired at various lift heights using the interleave scan mode as previously described.[6,25] As a control, samples were also imaged at various lift heights using a non-magnetic AFM probe (D-AFM) (NSC15, Mikromasch).

For ID-MFM, SPIONs were immobilized on side B (Fig. 1b) of commercially available silicon-nitride TEM windows of thickness 10 nm (SiMPore, Inc. SN100-A10Q33B), 20 nm (SiMPore Inc. SN100-A20Q05) or 50 nm (Silson Ltd. 11802114; DuraSiN DTF-05523). For this purpose, the silicon nitride windows were held *via* their silicon frame and suspended in air by using reverse-action self-closing tweezers so that neither side A nor side B was in contact with any surface. An aliquot (2 μL) of aqueous suspension of SPIONs was pipetted onto the window area on side

B and allowed to air dry overnight in ambient air. The silicon nitride windows were then adhered to a stainless-steel stub by using a double-sided scotch tape, with side B facing down towards the stub and side A exposed for scanning. The stubs were mounted onto the base of a JV scanner of the Multimode AFM. A reflected light module mounted over the AFM head enabled positioning of the probe on the silicon nitride window. Height and phase images were obtained by scanning the side A of the membrane using the tapping mode as described for D-MFM. All images for ID-MFM were acquired by using a MFM probe in the main mode (at zero lift height with no interleaved scanning). As a control, images were also acquired using a non-magnetic AFM probe in the indirect mode *i.e.* ID-AFM. At least $n = 3$ samples were tested per window thickness.

Quantitative analysis was performed to evaluate the signal strength from regions emanating MFM phase signal in both D-MFM and ID-MFM by using the section analysis feature of the Nanoscope software. In D-MFM, lift heights (z) of 10, 20 and 50 nm were utilized for comparison to the corresponding window thicknesses (t) in ID-MFM experiments. ID-AFM and ID-MFM measurements were also conducted on $n = 3$ nascent membranes to evaluate the level of noise in height and phase signals across two random points (separated ~1 μm apart) in the corresponding images. At least $n = 10$ measurements were made to ascertain the average noise values. Student's two-tailed unpaired t-test was used to ascertain statistically significant differences across the samples. A p-value < 0.05 was considered significant.

Multimodal microscopy

Fluorescence microscopy and bright field TEM were performed on the very same silicon nitride TEM windows (prepared as described above) before and after subjecting them to ID-MFM analysis, respectively. Fluorescence microscopy was performed using a Zeiss Axiovert 200 microscope equipped with appropriate filter cubes and a Hamamatsu camera. Bright field TEM imaging was performed using a JOEL JEM 1400 TEM (JOEL USA, Peabody, MA) operating at 80 kV and imaged using a Veleta digital camera (EMSIS). FIJI ImageJ was used to measure the width (diameter) of the SPIONs in TEM images.

Results

Characterization of SPIONs

The fluorescently-conjugated SPIONs used in this study were characterized using SQUID magnetometry, fluorescence microscopy and transmission electron microscopy (TEM). As

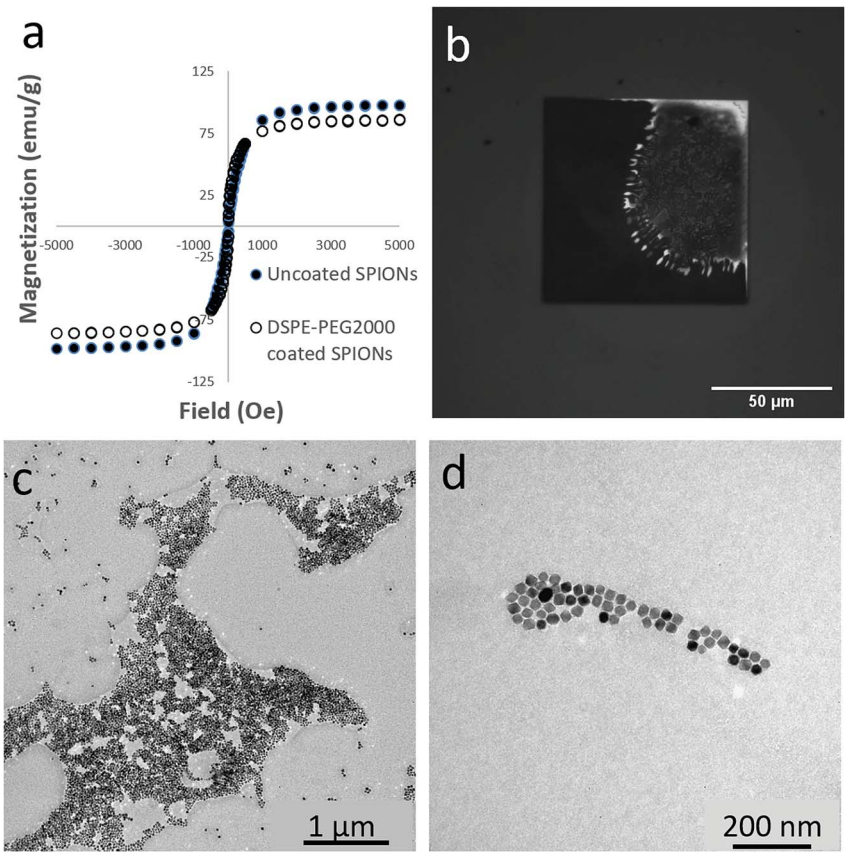

Fig. 2 (a) SQUID magnetometry of superparamagnetic iron oxide nanoparticles (SPIONs) with and without DSPE-PEG2000 coating as indicated. Magnetization curves were acquired by dispersing uncoated SPIONs in hexatriacontane (wax) and DSPE-PEG2000 coated SPIONs in gypsum. Measurements were taken at room temperature from −0.5 to 0.5 T. (b) Fluorescence microscopy of a silicon nitride window with DSPE-PEG2000 coated SPIONs immobilized on side B. (c) TEM image of silicon nitride window with DSPE-PEG2000 coated SPIONS on side B. Irregular shaped regions (several microns in size) consisting of dense clusters of SPIONs as well as smaller clusters (as shown in (d)) were observed.

shown by SQUID magnetometry measurements in Fig. 2a, the SPIONs had a negligible remnant magnetization at room temperature, characteristic of their superparamagnetic behavior. As-synthesized uncoated SPIONs had a saturation magnetization of 98 emu g^{-1} Fe, which is close to the saturation magnetization of bulk magnetite (127 emu g^{-1}). The DSPE-PEG 2000 coated SPIONs displayed a similar superparamagnetic behavior with a saturation magnetization of 86 emu g^{-1}.

Fluorescence microscopy was performed prior to ID-MFM analysis to confirm the presence of SPIONs immobilized on side B of silicon nitride windows. As shown in Fig. 2b, the fluorescence signal from aggregates of DSPE-PEG2000 SPIONs could be easily detected using fluorescence microscopy. Empty (nascent) windows showed no fluorescence signal (data not shown). Bright field TEM was used to determine the size of SPIONs and their surface coverage on the very same silicon nitride windows after ID-MFM analysis. As shown in Fig. 2c and d, SPIONs were dispersed on the silicon nitride windows in varying degrees of aggregation ranging from densely packed regions several microns in size to smaller clusters and monodispersed particles. The regions with dense clusters of SPIONs were irregular in size and shape and heterogeneous in particle density. Particle size measurements from TEM images indicated that SPIONs were fairly uniform in size with an average diameter of 16.0 ± 1.9 nm.

Magnetic force microscopy

To establish the feasibility of ID-MFM, height and phase images were acquired on side A of the silicon nitride windows with SPIONs immobilized on side B by using magnetic (MFM) as well as non-magnetic (AFM) probes. Fig. 3 shows how the AFM and the MFM probe, when used in indirect mode on windows t = 10 nm in thickness, detected regions which exhibited a topographical height. These regions were several microns in size

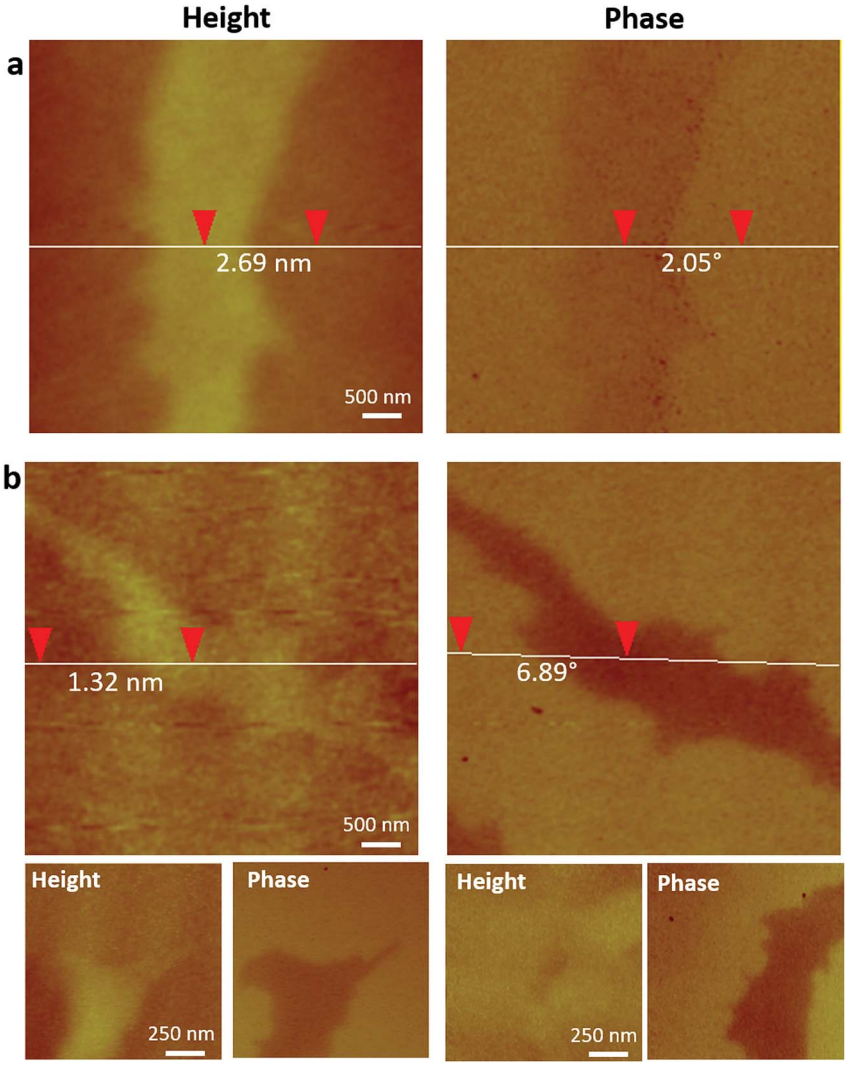

Fig. 3 ID-AFM and ID-MFM on 10 nm thick silicon nitride windows with DSPE-PEG2000 coated SPIONs immobilized on side B. Topography and phase images were acquired on side A using (a) an AFM probe and (b) an MFM probe. Vertical distance between two points obtained using section profile is indicated on height and phase images in (a) and (b). Bottom row in (b) shows height and corresponding phase image of two additional regions imaged using ID-MFM. Additional regions imaged using ID-AFM are shown in Fig. S1.†

and had irregular morphology, very similar to that observed for aggregates of SPIONs in our TEM images. The average topographic height of these regions for ID-MFM and ID-AFM were 3.8 ± 0.97 nm and 2.4 ± 0.61 nm with no statistically significant differences between them. The topographical height thus measured was significantly less than the size of single SPION and likely resulted due to a minor deformation of the window. Thus, our results reveal that although some topographical artifacts were observed in ID-MFM and ID-AFM modes at $t =$ 10 nm, they did not correspond to the true topography of the sample, which is expected as the sample was shielded by a silicon nitride window.

Analysis of phase signals in ID-MFM experiments revealed a distinct negative phase shift (above the noise level) which corresponded to the irregular shaped regions observed in height images. Such a phase shift was observed only when using an MFM probe and a negligible or undetectable signal (below noise level) was obtained in the ID-AFM mode (Fig. 3 and S1†). When the window thickness was increased to $t = 20$ nm, almost no topographical height could be detected from the SPION samples in ID-AFM or ID-MFM mode (Fig. 4). However, irregularly shaped regions similar to that observed at $t = 10$ nm exhibited a negative phase shift in ID-MFM at $t = 20$ nm with no signal in the ID-AFM mode (Fig. S1†). Increasing the window thickness to $t = 50$ nm resulted in a loss of both the topographical height as well as phase shift signals from all samples in both ID-AFM and ID-MFM modes (Fig. S2†). Thus, our analysis indicated that ID-MFM could detect negative phase shifts from regions with clusters of SPIONs through $t = 10$ and 20 nm windows. We did not observe a distinguishable phase shift which could be correlated to the size of mono-disperse SPIONs in ID-MFM at any window thickness.

To compare our ID-MFM measurements with the conventional D-MFM, we performed D-MFM on SPIONs immobilized

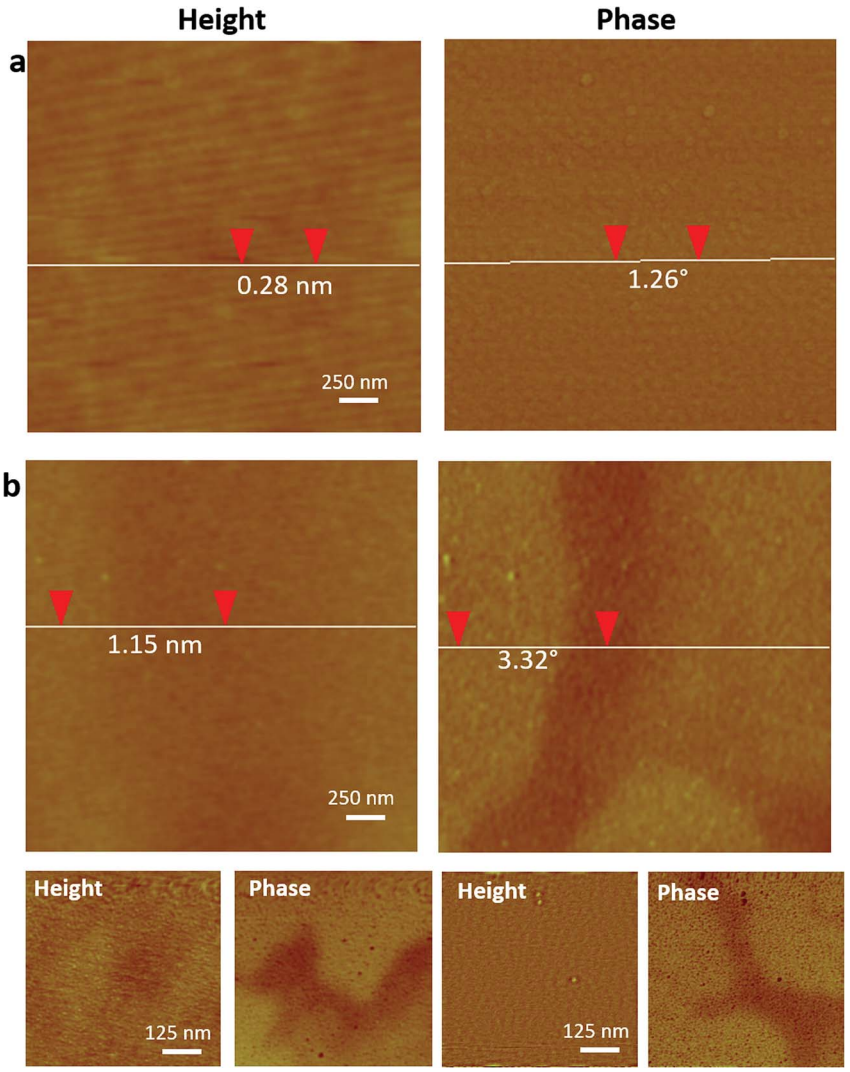

Fig. 4 ID-AFM and ID-MFM on 20 nm thick silicon nitride windows with DSPE-PEG2000 coated SPIONs immobilized on side B. Topography and phase images were acquired on side A using (a) an AFM probe and (b) an MFM probe. Vertical distance between two points obtained using section profile is indicated on height and phase images in (a) and (b). Bottom row in (b) shows height and corresponding phase image of two additional regions imaged using ID-MFM. Additional regions imaged using ID-AFM are shown in Fig. S1.†

on a mica surface at various lift-heights (z). As shown in Fig. 5, irregular regions with aggregates of SPIONs could be easily identified in topographical height images with both AFM and MFM probes. These regions in D-AFM and D-MFM images exhibited a height profile of 20.8 ± 2.63 nm and 18.0 ± 1.30 nm, respectively. This was significantly higher than that observed in our ID-MFM experiments ($p < 0.05$). When scanned at various lift heights above the sample, only D-MFM yielded a clearly detectable negative phase shift for $z \geq 10$ nm to over 50 nm with minimal signal in the D-AFM mode.

Qualitative analysis of height and phase images enabled us to compare signals in D-MFM and ID-MFM modes. As shown in Fig. 6a, the topographic height of aggregates of SPIONs was significantly higher in D-MFM and D-AFM as compared to ID-MFM and ID-AFM modes. Interestingly the phase signal revealed no significant difference ($p > 0.05$) across D-MFM and ID-MFM when compared at similar z or t values (Fig. 6b). As expected, both the D-MFM and ID-MFM showed a decrease in the magnitude of phase signal as the probe sample distance (z) or the membrane thickness (t) was increased from 10 to 20 nm. At $z = 50$ nm, D-MFM phase signal was further reduced to $1.65 \pm 0.44°$. However, at $t = 50$ nm ID-MFM failed to detect a topographic height corresponding to aggregates of SPIONs and the measured phase signals from randomly selected regions could not be distinguished above the noise level.

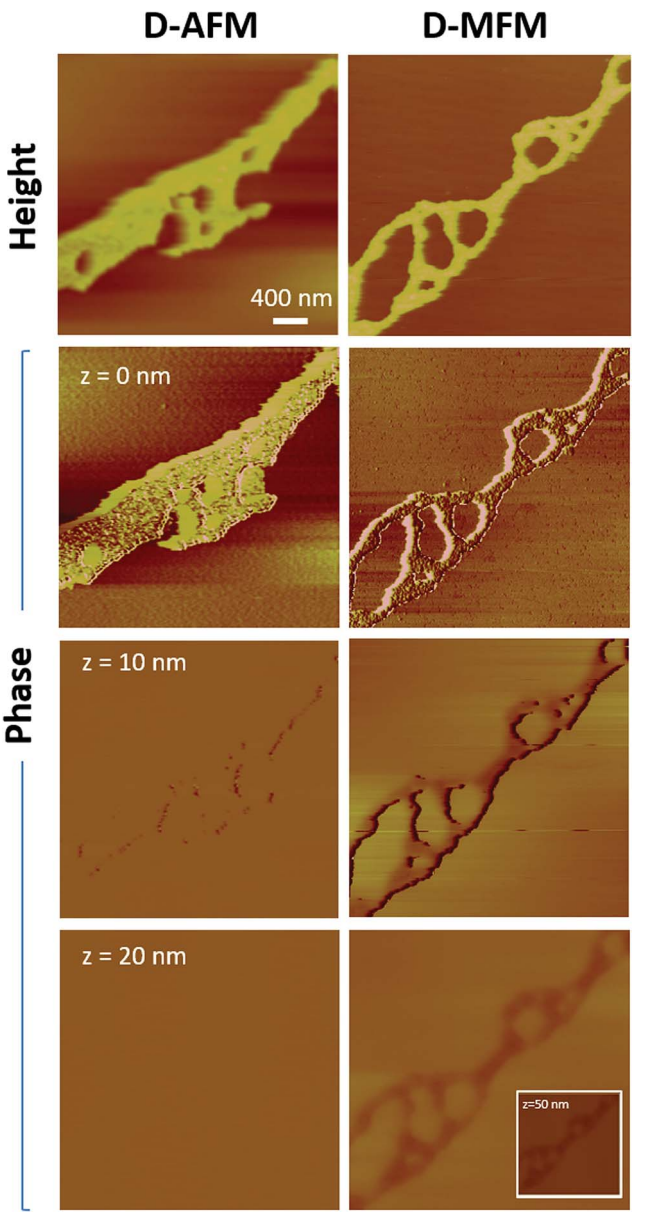

Fig. 5 D-MFM images of clusters of DSPE-PEG2000 coated SPIONs immobilized on a mica surface using an AFM and MFM probe as indicated. First row represents the height image and subsequent rows represent phase images of the same region acquired at increasing lift heights (z) as indicated.

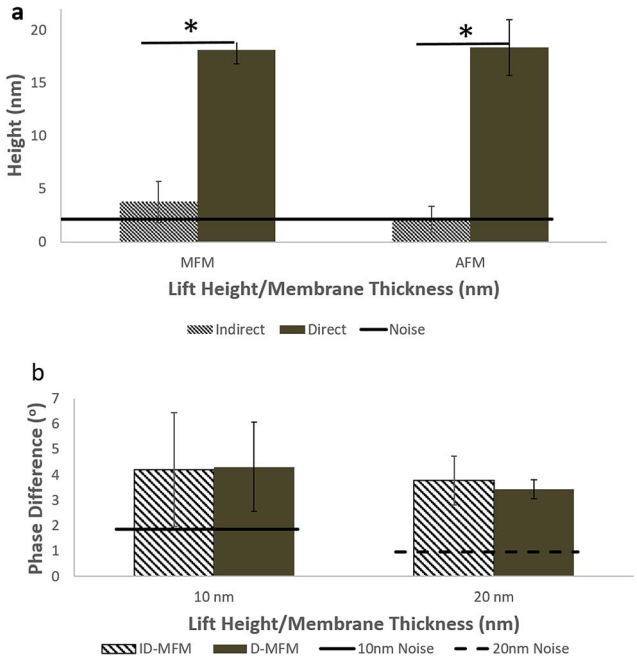

Fig. 6 (a) Comparison of topographic heights obtained in direct and indirect MFM and AFM modes from clusters of DSPE-PEG2000 coated SPIONs immobilized on a mica surface (for D-AFM/MFM) and 10 nm thick silicon nitride windows (for ID-AFM/MFM). (b) Comparison of phase signal between ID-MFM and D-MFM at equivalent lift heights (z) and window thickness (t) of 10 and 20 nm. The noise line is estimated by random measurements from images of nascent windows.

Discussion

We demonstrate here the feasibility of a novel ID-MFM technique to detect SPIONs through a silicon nitride window. While multiple scans at various lift-heights were obtained in D-MFM mode, only a single scan was needed in ID-MFM mode without the need to lift the probe from the window surface. A negative phase shift could be detected for aggregates of SPIONs in both D-MFM and ID-MFM mode. This is expected, as in our experiments the MFM probe was used to both induce and detect magnetic moments in the SPIONs, which results in an attractive magnetic force between the probe and the SPIONs. The magnitude of the MFM signal was not significantly affected by the presence of the silicon-nitride window as both the D-MFM

and ID-MFM exhibited similar phase shifts at similar probe-sample separations of 10 or 20 nm. Our observation that silicon nitride window does not dampen the MFM signal is consistent with other reports where silicon nitride coatings have been utilized to protect magnetic memory devices,[26] without affecting their magnetic read/write capabilities. In addition, magnetic micro-particles have been successfully manipulated through a silicon nitride window *via* an MFM probe.[27]

It should be noted that spatial resolution and sensitivity of MFM is governed not only by the size of the magnetic domain(s) but also their magnetic moment. Our results show that we could primarily detect aggregates of SPIONs in ID-MFM mode. This is explicable as aggregation of SPIONs has been demonstrated to increase their overall magnetization and the MFM signal due to enhanced magnetic dipole interactions.[4,10,28] While we could not detect mono-dispersed SPIONs using ID-MFM in this study, it is possible that particles with a higher magnetic moment (*e.g.* ferromagnetic particles) may be detectable using ID-MFM at the single particle level. Another factor which could influence the sensitivity of ID-MFM would be the surface roughness of the silicon nitride window which contributes to the noise level in height and phase images. As shown in our studies, although D-MFM detected a weak signal at probe-sample separation of 50 nm, no distinct signal could be detected using ID-MFM on a 50 nm thick window as the weak signal was below the noise level of ID-MFM. Use of windows with a smoother topography and minimized surface roughness may help enhance the sensitivity of ID-MFM. Nevertheless, MFM studies of aggregates of SPIONs holds relevance for several applications.[4,10,11,28] Further, in biological samples, naturally present ferritin (iron) deposits are aggregated in lysosomal structures,[18] in a manner similar to SPIONs aggregates.

We also elucidate how ID-MFM is amenable to multi-modal microscopy as the silicon nitride windows utilized in ID-MFM are transparent to light and electron optics.[29] By using DSPE-PEG2000 coated SPIONs, we could detect aggregates of SPIONs using wide-field fluorescence microscopy. Further, the very same windows could be imaged using TEM. These multi-modal approaches enabled us to confirm the accumulation of SPIONs on the silicon nitride TEM grids. The size, shape, and heterogeneity in the density of regions comprised of SPIONs aggregates in TEM images matched that of the regions exhibiting ID-MFM signal. Recent years have witnessed a rise in multi-functional magnetic nanoparticles for various applications.[30] Such particles could benefit by characterization and detection using the multimodal ID-MFM.

In our experience, the ID-MFM technique presented its own issues, particularly with sample preparation. Due to ultrathin nature of window required for ID-MFM, the silicon nitride windows were susceptible to rupture during handling. Further, although we did not expect any topographic signal in ID-MFM, a small topographic feature was observed when the window thickness was 10 nm, indicating that the window can deform due to sample immobilization. The TEM windows utilized in this study are designed to mount the sample on side A, *i.e.* the exposed surface of the silicon nitride window. For ID-MFM we had to disperse the sample on side B through a 200 to 500 μm deep well onto a tiny window (typically less than 1.0 × 1.0 mm), which limited our ability to blot or wash off the excess sample and ensure a uniform coating of the SPIONs. Further work on custom-designed windows of optimized geometries and/or use of other materials for ultrathin windows[31] may be advantageous for ID-MFM.

Conclusions

We demonstrate here ID-MFM as a novel modality for high-throughput multimodal detection of magnetic domains which can be implemented using commercially available AFM equipment and probes. ID-MFM could be especially advantageous for biomedical applications to enable magnetic mapping of iron deposits in cells and tissue sections, without contaminating the probe. In recent years, electron microscopy[32] as well as MFM studies on samples maintained in a liquid environment have been gathering attention. In this regard, MFM in fluids has been achieved using D-MFM, but the resulting images suffer from artifacts,[33] require custom modifications in the mode of operation,[34] equipment accessories.[22] ID-MFM may offer an easier and more versatile approach to keep samples in a fluid environment. Further advances in the design of microfluidic platforms as well as MFM probes[35,36] would be required to enhance the capabilities of ID-MFM.

Conflicts of interest

There are no conflicts to declare.

Acknowledgements

This work was supported by a facility grant from the Institute of Materials Research at The Ohio State University and in part by the National Science Foundation (CBET award 1403574 to G. A.) and by the Cancer Prevention and Research Institute of Texas (RR140081 and RR170721 to G. B.).

References

1 G. Agarwal, in *Magnetic Nanomaterials for Life Sciences*, Wiley-VCH Verlag GmbH & Co. KGaA, 2009.
2 E. Pinilla-Cienfuegos, S. Mañas-Valero, A. Forment-Aliaga and E. Coronado, Switching the Magnetic Vortex Core in a Single Nanoparticle, *ACS Nano*, 2016, **10**, 1764–1770.
3 X. Batlle, *et al.*, Direct imaging of the magnetic polarity and reversal mechanism in individual $Fe_{3-x}O_4$ nanoparticles, *Nanoscale*, 2015, **7**, 8110–8114.
4 V. F. Puntes, P. Gorostiza, D. M. Aruguete, N. G. Bastus and A. P. Alivisatos, Collective behaviour in two-dimensional cobalt nanoparticle assemblies observed by magnetic force microscopy, *Nat. Mater.*, 2004, **3**, 263–268.
5 C. S. Neves, *et al.*, New insights into the use of magnetic force microscopy to discriminate between magnetic and nonmagnetic nanoparticles, *Nanotechnology*, 2010, **21**, 305706.

6 S. Schreiber, *et al.*, Magnetic force microscopy of superparamagnetic nanoparticles, *Small*, 2008, **4**, 270–278.
7 S. Sievers, *et al.*, Quantitative measurement of the magnetic moment of individual magnetic nanoparticles by magnetic force microscopy, *Small*, 2012, **8**, 2675–2679.
8 T. M. Nocera, J. Chen, C. B. Murray and G. Agarwal, Magnetic anisotropy considerations in magnetic force microscopy studies of single superparamagnetic nanoparticles, *Nanotechnology*, 2012, **23**, 495704.
9 L. Angeloni, *et al.*, Single nanoparticles magnetization curves by controlled tip magnetization magnetic force microscopy, *Nanoscale*, 2017, **9**, 18000–18011.
10 J. A. Fuentes-García, A. I. Diaz-Cano, A. Guillen-Cervantes and J. Santoyo-Salazar, Magnetic domain interactions of Fe_3O_4 nanoparticles embedded in a SiO_2 matrix, *Sci. Rep.*, 2018, **8**, 5096.
11 C. Moya, Ó. Iglesias-Freire, X. Batlle, A. Labarta and A. Asenjo, Superparamagnetic *versus* blocked states in aggregates of $Fe_{3-x}O_4$ nanoparticles studied by MFM, *Nanoscale*, 2015, **7**, 17764–17770.
12 D. Passeri, *et al.*, Magnetic force microscopy: Quantitative issues in biomaterials, *Biomatter*, 2014, **4**, e29507.
13 S. Hsieh, C. W. Hsieh and B. Zheng, Ferritin protein imaging and detection by magnetic force microscopy, *Chem. Commun.*, 2010, **46**, 1655–1657.
14 T. M. Nocera, Y. Zeng and G. Agarwal, Distinguishing ferritin from apoferritin using magnetic force microscopy, *Nanotechnology*, 2014, **25**, 461001.
15 K. J. Kim, H. Y. Cho, W. J. Lee and J. W. Choi, Subtyping of Magnetically Isolated Breast Cancer Cells Using Magnetic Force Microscopy, *Biotechnol. J.*, 2018, **13**, 1700625.
16 C. E. Diebel, R. Proksch, C. R. Green, P. Neilson and M. M. Walker, Magnetite defines a vertebrate magnetoreception, *Nature*, 2000, **406**, 299–302.
17 C. Marcuello, L. Chambel, M. S. Rodrigues, L. P. Ferreira and M. M. Cruz, Magnetotactic Bacteria: Magnetism beyond Magnetosomes, *IEEE Trans. Nanobioscience*, 2018, **17**, 555–559.
18 A. R. Blissett, B. Ollander, B. Penn, D. M. McTigue and G. Agarwal, Magnetic mapping of iron in rodent spleen, *Nanomedicine Nanotechnology, Biol. Med.*, 2017, **13**, 977–986.
19 A. R. Blissett, *et al.*, Sub-cellular *In situ* Characterization of Ferritin (iron) in a Rodent Model of Spinal Cord Injury, *Sci. Rep.*, 2018, **8**, 3567.
20 M. Jaafar, *et al.*, Distinguishing magnetic and electrostatic interactions by a Kelvin probe force microscopy-magnetic force microscopy combination, *Beilstein J. Nanotechnol.*, 2011, **2**, 552–560.
21 L. Angeloni, D. Passeri, M. Reggente, D. Mantovani and M. Rossi, Removal of electrostatic artifacts in magnetic force microscopy by controlled magnetization of the tip: Application to superparamagnetic nanoparticles, *Sci. Rep.*, 2016, **6**, 26293.
22 P. Ares, M. Jaafar, A. Gil, J. Gõmez-Herrero and A. Asenjo, Magnetic Force Microscopy in Liquids, *Small*, 2015, **11**, 4731–4736.
23 S. Tong, C. A. Quinto, L. Zhang, P. Mohindra and G. Bao, Size-Dependent Heating of Magnetic Iron Oxide Nanoparticles, *ACS Nano*, 2017, **11**, 6808–6816.
24 S. Tong, S. Hou, B. Ren, Z. Zheng and G. Bao, Self-assembly of phospholipid-PEG coating on nanoparticles through dual solvent exchange, *Nano Lett*, 2011, **11**, 3720–3726.
25 M. Savla, R. P. Pandian, P. Kuppusamy and G. Agarwal, Magnetic force microscopy of an oxygen-sensing spin-probe, *Isr. J. Chem.*, 2008, **48**, 33–38.
26 B. K. Yen, *et al.*, Microstructure and properties of ultrathin amorphous silicon nitride protective coating, *J. Vac. Sci. Technol., A*, 2003, **21**, 1895.
27 E. Mirowski, J. Moreland, A. Zhang, S. E. Russek and M. J. Donahue, Manipulation and sorting of magnetic particles by a magnetic force microscope on a microfluidic magnetic trap platform, *Appl. Phys. Lett.*, 2005, **86**, 243901.
28 B. Duong, *et al.*, Enhanced magnetism in highly ordered magnetite nanoparticle-filled nanohole arrays, *Small*, 2014, **10**, 2840–2848.
29 E. A. Ring, D. B. Peckys, M. J. Dukes, J. P. Baudoin and N. DE Jonge, Silicon nitride windows for electron microscopy of whole cells, *J. Microsc.*, 2011, **243**, 273–283.
30 E. S. Vasquez, J. M. Feugang, S. T. Willard, P. L. Ryan and K. B. Walters, Bioluminescent magnetic nanoparticles as potential imaging agents for mammalian spermatozoa, *J. Nanobiotechnology*, 2016, **14**, 20.
31 D. J. Kelly, *et al.*, Nanometer Resolution Elemental Mapping in Graphene-Based TEM Liquid Cells, *Nano Lett*, 2018, **18**, 1168–1174.
32 N. d. Jonge, D. B. Peckys, G. J. Kremers and D. W. Piston, Electron microscopy of whole cells in liquid with nanometer resolution, *Proc. Natl. Acad. Sci.*, 2009, **106**, 2159–2164.
33 R. Giles, *et al.*, Noncontact force microscopy in liquids, *Appl. Phys. Lett.*, 1993, **63**, 617–618.
34 C. Dietz, E. T. Herruzo, J. R. Lozano and R. Garcia, Nanomechanical coupling enables detection and imaging of 5 nm superparamagnetic particles in liquid, *Nanotechnology*, 2011, **22**(12), 125708.
35 V. Neu, S. Vock, T. Sturm and L. Schultz, Epitaxial hard magnetic SmCo5 MFM tips-a new approach to advanced magnetic force microscopy imaging, *Nanoscale*, 2018, **10**, 16881–16886.
36 Y. Cao, *et al.*, Magnetic domain structure imaging near sample surface with alternating magnetic force microscopy by using AC magnetic field modulated superparamagnetic tip, *Nanotechnology*, 2018, **29**, 305502.